SCIENTIFIC REPORTS

OPEN

SUBJECT AREAS:
MATERIALS FOR OPTICS
OPTICAL MATERIALS AND STRUCTURES
OPTICAL PHYSICS

Received
11 March 2014

Accepted
6 May 2014

Published
23 May 2014

Correspondence and requests for materials should be addressed to D.P.C. (dpchen@mail.siom.ac.cn)

Spectroscopic properties and energy transfer parameters of Er^{3+}- doped fluorozirconate and oxyfluoroaluminate glasses

Feifei Huang[1,2], Xueqiang Liu[1,2], Lili Hu[1] & Danping Chen[1]

[1]Key Laboratory of Materials for High Power Laser, Shanghai Institute of Optics and Fine Mechanics, Chinese Academy of Sciences, Shanghai 201800, PR China, [2]Graduate School of Chinese Academy of Sciences, Beijing 100039, PR China.

Er^{3+}- doped fluorozirconate (ZrF_4-BaF_2-YF_3-AlF_3) and oxyfluoroaluminate glasses are successfully prepared here. These glasses exhibit significant superiority compared with traditional fluorozirconate glass (ZrF_4-BaF_2-LaF_3-AlF_3-NaF) because of their higher temperature of glass transition and better resistance to water corrosion. Judd-Ofelt (J-O) intensity parameters are evaluated and used to compute the radiative properties based on the VIS-NIR absorption spectra. Broad emission bands located at 1535 and 2708 nm are observed, and large calculated emission sections are obtained. The intensity of 2708 nm emission closely relates to the phonon energy of host glass. A lower phonon energy leads to a more intensive 2708 nm emission. The energy transfer processes of Er^{3+} ions are discussed and lifetime of Er^{3+}: $^4I_{13/2}$ is measured. It is the first time to observe that a longer lifetime of the $^4I_{13/2}$ level leads to a less intensive 1535 nm emission, because the lifetime is long enough to generate excited state absorption (ESA) and energy transfer (ET) processes. These results indicate that the novel glasses possess better chemical and thermal properties as well as excellent optical properties compared with ZBLAN glass. These Er^{3+}- doped ZBYA and oxyfluoroaluminate glasses have potential applications as laser materials.

Rare-earth elements are of interest in several high-tech and environmental applications[1–6]. Over the past decades, Er^{3+} has become one of the most interesting centers of research because of its 1.55 and 2.7 μm emissions from $^4I_{13/2} \rightarrow {}^4I_{15/2}$ and $^4I_{11/2} \rightarrow {}^4I_{13/2}$ transitions, respectively[4,7–11]. The Er^{3+}- doped fiber amplifier is one of the important devices used in the 1.5 μm wavelength optical communication window. Er^{3+} waveguide laser and up-conversation laser operations have been achieved at room temperature[12]. The optical properties of Er^{3+} are interesting because of their applications in infrared lasers operating at eye-safe wavelengths[8,13]. 2.7 μm emission is also becoming a concern for researchers owing to the strong absorption of radiation by water. It has potential applications in medicine, sensing, and military countermeasures, as well as in light detection and ranging[14,15]. Meanwhile, the maturity of laser diodes (LDS) accelerates Er^{3+} development because of its efficient absorption at 800 or 980 nm.

Glasses known as convenient hosts for rare earth ions have been widely used because of their good mechanical and thermal stability, low synthesis cost, as well as possibility of pulling to fiber[16]. Er^{3+}- doped fluoride, chalcogenide, fluorophosphate, silicate, and heavy metal oxide (tellurite, germanate, and bismuthate) glasses have been investigated for applications in near- and mid-infrared (IR) regions[14,17]. Fluoride glasses are potential candidates for Er^{3+} doped materials because of their low phonon energy and wide optical transmission window, ranging from UV to mid-IR[18,19]. The fluorozirconate system, notably the ZrF_4-BaF_2-LaF_3-AlF_3-NaF (ZBLAN) glass composition, is one of the most stable systems against devitrification among fluoride glasses. However, Er^{3+}: ZBLAN fiber lasers have poor thermal properties (i.e., very low melting temperatures and high heat generation of Er^{3+} actives ions) compared with those of near-IR silica-based fiber lasers, and the relatively large loss of ZBLAN fibers limits the usable length of the fibers, so further scaling up the power output is fundamentally difficult[20,21]. Thus, exploring effective fluoride glasses for host matrices becomes a challenge to researchers, for example the fluorozirconate system (ZBYA)[22].

Fluoroaluminate glasses (AlF_3-based glasses) have better chemical durability and enhanced mechanical strength than fluorozirconate glasses, which would thus be useful for optical applications[23]. However, some

devitrification problems are associated with these glasses. The addition of some oxides, especially $Al(PO_3)_3$ or TeO_2, is effective to stabilize the glass state[24]. Oxyfluoroaluminate glasses containing low P or Te have potential applications as hosts for high-power glass lasers.

Several structural studies have revealed the basic structure of these glasses (ZBYA and oxyfluoroaluminate glasses)[22,25]. However, few investigations are available on the thermal, chemical, and the 1.5 and 2.7 μm emissions properties of these Er^{3+}- doped glasses. In this study, fluorozirconate glass (ZBYA) and oxyfluoroaluminate glasses containing low P or Te are successfully prepared. The thermal and chemical properties of these glasses are investigated. The absorption and emission spectra at near- and mid-IR regions are tested. Simultaneously, the spectroscopic properties, Judd-Ofelt theory analysis results, cross sections, and emission parameters of these glasses are discussed.

Experimental

The compositions of the glasses were ZrF_4-BaF_2-YF_3-AlF_3-$1ErF_3$ (designated as ZBYA), $99(AlF_3$-YF_3-CaF_2-BaF_2-SrF_2-$MgF_2)$–$1Al(PO_3)_3$–$1ErF_3$ (designated as AYFP or FP) and $90(AlF_3$-YF_3-CaF_2-BaF_2-SrF_2-$MgF_2)$–$10TeO_2$–$1ErF_3$ (designated as AYFT or FT). For comparison, fluorozirconate glass with composition of $100(ZrF_4$-BaF_2-LaF_3-AlF_3-$NaF)$–$1ErF_3$ (designated as ZBLAN) was prepared. The samples were prepared using high-purity ZrF_4, AlF_3, YF_3, CaF_2, BaF_2, SrF_2, MgF_2, $Al(PO_3)_3$, TeO_2 and ErF_3 powders. Well-mixed 25 g batches of the samples were placed in platinum crucibles and melted at about 1100°C for 30 min. Then the melts were poured onto a preheated copper mold and annealed in a furnace around the glass transition temperature. The annealed samples were fabricated and polished to the size of 20 mm × 15 mm × 1 mm for the optical property measurements.

The characteristic temperatures (temperature of glass transition T_g and temperature of onset crystallization peak T_x) of the samples were determined using a NetzschSTA449/C differential scanning calorimetry at a heating rate of 10 K/min. The densities and refractive indices of the samples were measured through the Archimedes method using distilled water as an immersion liquid and the prism minimum deviation method respectively. Furthermore, the absorption spectra were recorded with a Perkin-Elmer Lambda 900 UV/VIS/NIR spectrophotometer in the range of 300 nm to 1600 nm, and the emission spectra were measured with a Triax 320 type spectrometer (Jobin-Yvon Co., France). All the measurements were carried out at room temperature.

Results and discussion

Differential scanning calorimeter results. Fig. 1 shows the DSC results of the four samples in this study. Characteristic temperatures of T_g (temperature of glass transition), T_x (temperature of onset of crystallization), and T_p (temperature of peak of crystallization) are also marked in Fig. 1. T_g is an important factor for laser glass, higher values of the oxyfluoroaluminate glasses compared with those of fluorozirconate glasses and other reported glasses[26] give glass good thermal stability to resist thermal damage at high pumping intensities. The glass criterion, $\Delta T = T_x - T_g$ introduced by Dietzel[27,28], is often regarded as an important parameter for evaluating the glass forming ability. ΔT has been frequently used as a rough criterion to measure glass thermal stability. A large ΔT indicates strong inhibition of nucleation and crystallization. The glass formation factor of the materials is given by the parameter $k_{gl} = (T_x - T_g)/(T_m - T_g)$, where T_m is the melting temperature of the glass[29]. Compared with ΔT, the parameter is more suitable in estimating the glass thermal stability. A larger k_{gl}, imparts better forming ability of the glass. The glass forming ability can be estimated by these given characteristic temperatures. The existing stability criterion parameters ΔT and k_{gl} of the samples are shown in Table 1. These values are larger than those of fluoride and phosphate glasses[30,31]. These results indicate that the ZBYA and oxyfluoroaluminate glasses have better forming ability and thermal stability against crystallization.

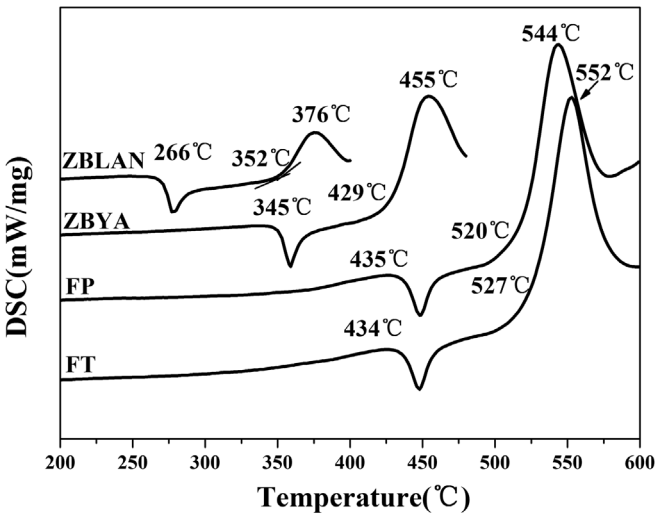

Figure 1 | DSC curves of the present samples.

Chemical stability. The chemical durability of the sample was measured as follows: First, the weighed sample (W_1) was placed into the distilled water. Second, the sample was kept in a thermostatic water bath at 98°C for 1 h and then cooled and dried in a dying box at 70°C for 1 h. Finally, the dry sample was weighed again (W_2). The chemical durability of glasses was evaluated using the value of $\Delta W\% = \frac{W_1 - W_2}{W_1} \times 100\%$[21]. The boiled water treatment process was repeated five times for each sample in this research. The results of the ΔW% are shown in Table 1. ZBLAN exhibits poorer resistance to water corrosion compared with the other samples, which coincides with the reported phenomenon[32].

The transmittance spectra of the samples before and after water treatment are shown in Fig. 2. Figure 2(a) shows the transmittance spectra of the samples without any treatment. Transmittance can reach as high as 90%, whereas approximately 10% loss contains the Fresnel reflection dispersion, and glass absorption. The fluorozirconate glasses have a weak absorption band at about 4500 nm because

Table 1 | Physical, thermal, and chemical parameters of the present glasses

				ΔW (mg/g)						
	ρ (g/cm³)	N (×10⁻²⁶/cm³)	n	1 h	2 h	3 h	4 h	5 h	ΔT(°C)	k_{gl}
ZBYA	4.55	1.35	1.502	0	0	0	0.66	0	82	0.324
ZBLAN	4.38	1.46	1.499	38.0	6.9	11.1	3.8	9.1	86	0.257
FP	3.81	2.14	1.431	0	0	0	0.91	0.45	85	0.183
FT	3.94	2.13	1.482	0	0	0	0	0	93	0.254

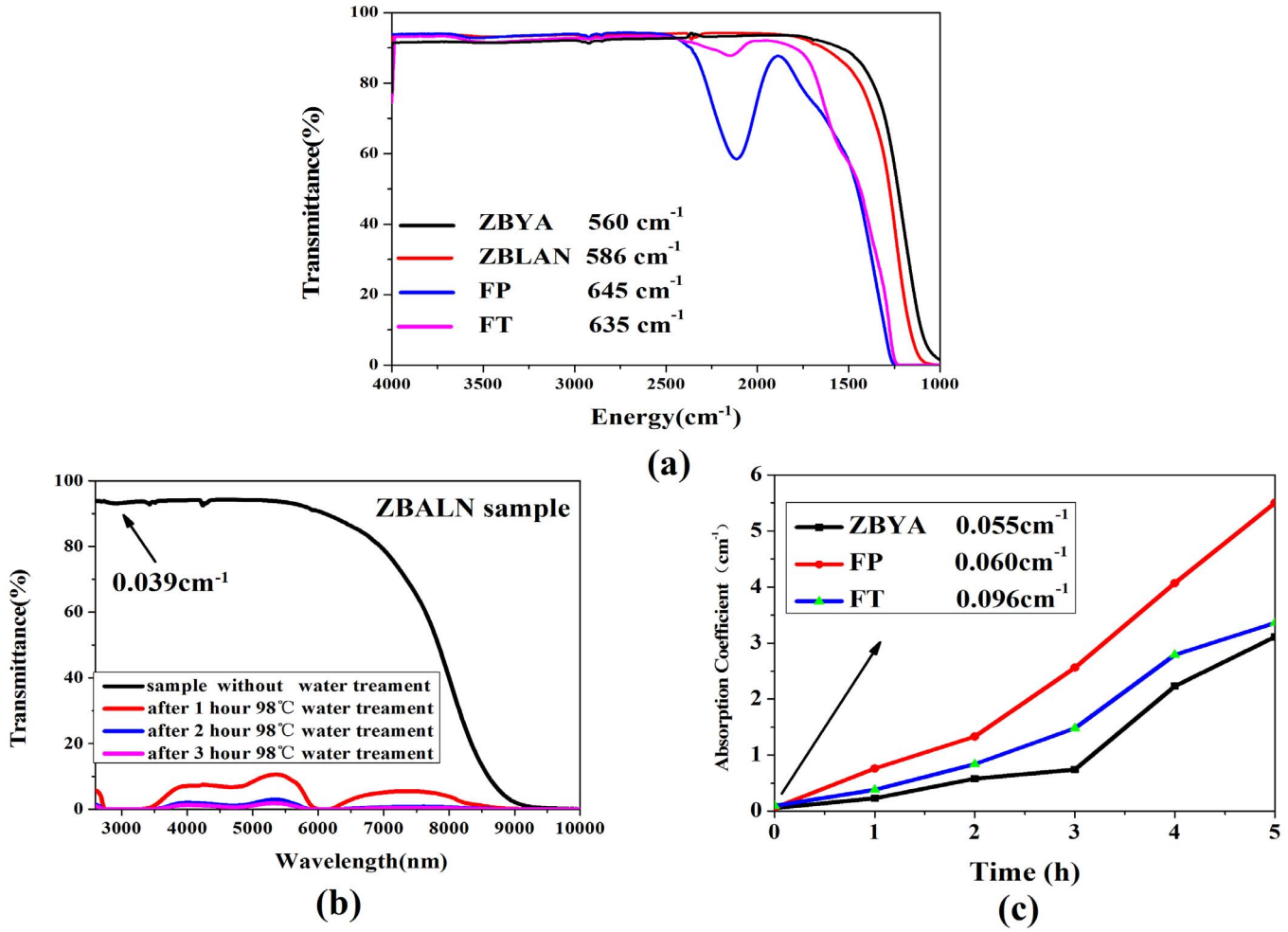

Figure 2 | Transmittance spectra of the present glasses before and after water treatment (a) Transmittance spectra of all the samples before treatment (b) Transmittance spectra of ZBLAN after treatment (c) The curves of OH^- absorption coefficient of the ZBYA, FP and FT samples depend on the treatment time.

of CO_2 absorption, and the oxyfluoroaluminate glasses possess an absorption band at about 4750 nm because of the vibration peak [XO]. However, these fluctuations do not influence the near- and mid-infrared emissions of Er^{3+}. The phonon energy can be inferred from the transmittance spectra, and large phonon energy increases the nonradiative decay rate. A higher nonradiative decay rate results in fewer radiative transitions and therefore less intense fluorescence bands[33]. The phonon energy calculated by this model is also presented in Figure 2 (a). ZBYA glass has the smallest phonon energy and the IR cut-off wavelength is at about 7 μm.

The transmittance spectra of the samples after water treatment are shown in Figures 2(b) and 2(c). The basic form of the spectra almost remains the same for ZBYA, FP, and FT samples. Only the absorption band at about 2900 nm caused by OH^- obviously changes. The OH^- in glass is related to the emission efficiency of rare-earth ions, because the residual OH^- groups will participate in the energy transfer of rare-earth ions and reduce the intensity of emissions[10,20]. The OH^- group content in the glass can be expressed by the absorption coefficient of the OH^- vibration band at 3 μm, which can be given by

$$\alpha_{OH^-} = \ln(T/T_0)/1 \qquad (1)$$

where l is the thickness of the sample, T_0, and T are the transmitted and incident intensities respectively. Figures 2(c) describes the relationship between the OH^- absorption coefficient and the time of water treatment for ZBYA, FP, and FT samples. The OH^- absorption coefficients of the original samples are 0.055, 0.060, and 0.096 cm^{-1}, respectively, which are significantly lower than some reported values of bismuthate glass[17], germanate glass[29], and fluorophosphates glass[34]. Some lower OH^- content glasses have also been reported[35] recently and it is reported that the OH^- absorption coefficient should be < 2 cm^{-1} to achieve optimum laser performance[34]. The values of the present glasses are far less than 2 cm^{-1}. Therefore, excellent transmission property provides these Er^{3+}- doped glasses with potential applications as laser materials. The OH^- absorption coefficient becomes larger for all the samples with increasing water treatment time, and ZBYA glass possesses best chemical stability according to Fig. 2(c). The ZBLAN sample has poor resistance to water corrosion. The spectra for the ZBLAN sample after water treatment are demonstrated alone in Fig. 2(b). After 1 h water treatment, the transmittance noticeably declines and the OH^- absorption coefficient approaches near infinity. Afterward, the ZBLAN glass becomes opaque at the mid-IR region.

Absorption spectra and calculation of optical parameters. Fig. 3 indicates the absorption spectra of the samples at room temperature in the wavelength region of 300 nm to 1600 nm. Absorption bands corresponding to the transitions starting from the $^4I_{15/2}$ ground state to the higher levels $^4I_{13/2}$, $^4I_{11/2}$, $^4I_{9/2}$, $^4F_{9/2}$, $^4S_{3/2}$, $^2H_{11/2}$, and $^4F_{7/2}$ are labeled. The shape and peak positions of each transition for the Er^{3+}-doped glasses are very similar to those of other Er^{3+}- doped glasses[36], indicating homogeneous incorporation of the Er^{3+} ions in the glassy network without clustering and changes in the local ligand field. The

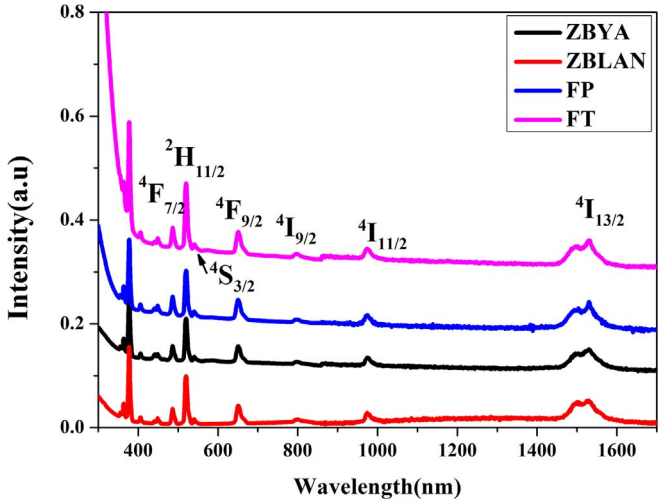

Figure 3 | Absorption spectra of the present samples.

absorption band around 980 nm indicates that these glasses can be efficiently excited by 980 nm LD.

Important spectroscopic and laser parameters of rare earth doped glasses have been commonly analyzed using the Judd–Ofelt theory[37,38]. Details of the theory and method have been well described earlier, so only the results will be presented in this section. The intensity parameters Ω_t of these Er^{3+}- doped glasses are calculated and shown in the Table 2. δ presents the agreement between calculated and experimental values. The room-mean-square error deviation of intensity parameters is $\times 10^{-6}$, which indicates the validity of the Judd-Ofelt theory for predicting the spectral intensities of Er^{3+} and the reliability of the calculations. Previous studies have revealed that Ω_2 parameters are indicative of the amount of the covalent bond, and are strongly dependent on the local environment of the ion sites, whereas the Ω_6 parameter is related to the overlap integrals of the *4f* and *5d* orbits[39]. Values of Ω_4 and Ω_6 also provide some information on the rigidity and viscosity of the hosts. However, compared with Ω_2, which bears higher sensitivity to the chemical nature of the hosts, structural information carried by Ω_4 and Ω_6 values is marginal and sometimes inaccurate. An analysis of the values of Ω_2 shows that the FP sample possesses lower covalence and higher symmetry. Compared with oxide glasses[18], fluoride glasses have smaller Ω_2 because an O^{2-} ion possesses higher polarizability than an F^- ion.

The calculated predicted spontaneous transition probability (A), branching ratio (β) and radiative lifetime (τ_{rad}) of certain optical transitions for Er^{3+}- doped fluoride glasses are also shown in Table 2. The predicted spontaneous emission probabilities of Er^{3+}: $^4I_{13/2} \rightarrow {}^4I_{15/2}$ and $^4I_{112} \rightarrow {}^4I_{13/2}$ transitions are presented, which are much higher than reported values[40]. Higher spontaneous emission probability provides a better opportunity to obtain laser actions.

Fluorescence properties and energy transfer processes. Under 980 nm diode laser excitation, the $^4I_{13/2} \rightarrow {}^4I_{15/2}$ fluorescence around 1.5 μm and $^4I_{11/2} \rightarrow {}^4I_{13/2}$ fluorescence around 2.7 μm are obviously observed, as seen in Fig. 4. For the present samples, no shift in the wavelength of the emission peaks is observed, but the peak intensity is evidently different. Generally, the intensity of 1530 nm is opposite of that of 2710 nm for the same sample in this study. The fluorozirconate glasses possess more intensive 2708 nm emission owing to the lower phonon energy. The multi-phonon nonradiative decay rate is given by the well-known energy gap law[41]

$$W_n = W_0[1 - \exp(-h\nu/kT)]^{-n} \quad (2)$$

where W_n is the rate at temperature T, W_0 is the rate at 0 K, n = ΔE/hν, ΔE is the energy gap between the levels involved, ν is the relevant

Table 2 | J-O parameters of Ω_t, radiative transition probability A_{rad}, branching ratio β, and lifetime of some selected levels τ_R of the present samples

Level		ZBYA			ZBLAN			FP			FT		
Initial level	End level	A_{rad} (S^{-1})	β	τ_R (ms)	A_{rad} (S^{-1})	β	τ_R (ms)	A_{rad} (S^{-1})	β	τ_R (ms)	A_{rad} (S^{-1})	β	τ_R (ms)
$^4I_{13/2}$	$^4I_{15/2}$	146.65	100%	6.82	155.21	100%	6.44	89.55	100%	11.17	122.73	100%	8.15
$^4I_{11/2}$	$^4I_{15/2}$	142.99	83.91%	5.87	152.88	84.15%	5.50	70.61	79.67%	11.28	115.92	83.11%	7.17
	$^4I_{13/2}$	27.41	16.09%		28.80	15.85%		18.02	20.33%		23.55	16.89%	
$^4I_{9/2}$	$^4I_{15/2}$	68.04	57.13%	8.4	85.01	60.97%	7.17	76.33	74.21%	9.72	59.18	59.25%	10.01
	$^4I_{13/2}$	49.04	41.18%		52.41	37.59%		24.79	24.10%		38.77	38.81%	
	$^4I_{11/2}$	2.01	1.69%		2.01	1.44%		1.74	1.69%		1.93	1.93%	
Ω (2,4,6)($\times 10^{-20}$)		3.01, 1.03, 1.64			3.27, 1.3, 1.75			1.53, 1.39, 0.95			3.1, 0.94, 1.35		
		δ 0.2 × 10^{-6}			0.29 × 10^{-6}			0.04 × 10^{-6}			0.15 × 10^{-6}		

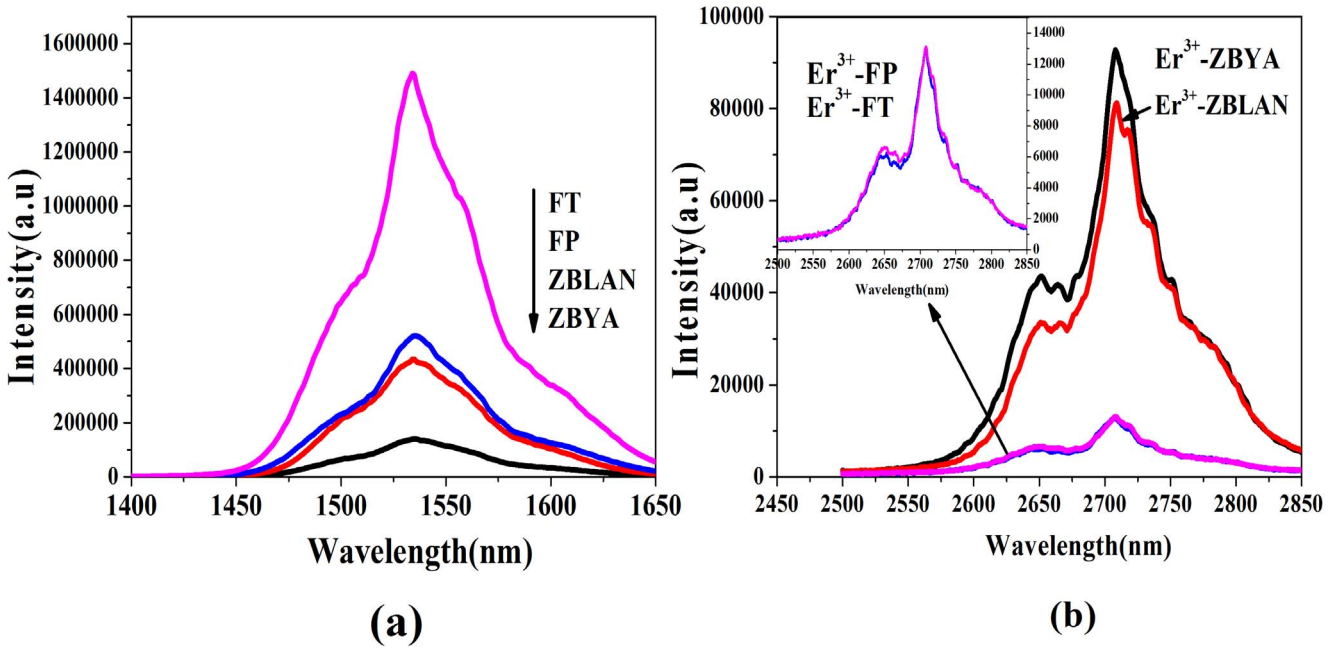

Figure 4 | **Emission spectra of the prepared samples: (a) 1.5 μm (b) 2.7 μm.**

phonon's frequency. When ΔE is equal to or less than 4–5 times the high-energy phonons, the multi-phonon nonradiative relaxation with the emission of a few high-energy phonons becomes competitive with radiative processes. The energy gap between the $^4I_{11/2}$ and $^4I_{13/2}$ levels is about 3690 cm^{-1}, which is equal to 5–6 times the high-energy phonons of the oxyfluoroaluminate glasses and 6–7 times that of the fluorozirconate glasses. The multi-phonon nonradiative relaxation with the 2.7 μm emission of the oxyfluoroaluminate glasses has a larger probability than that of the fluorozirconate glasses, which leads to a much lower intensity of the 2.7 μm emission. The higher intensity of the 1.5 μm emission of the oxyfluoroaluminate glasses can be explained by the $^4I_{13/2}$ level decay lifetime of the samples, which will be discussed below.

The upconversion spectra of the present samples are shown in Fig. 5(a). In this region, the green emissions at about 545 and 550 nm dominate. The green emission of the fluorozirconate glasses is stronger than that of the oxyfluoroaluminate glasses, which is similar to the emission of 2710 nm and opposite to that of the 1530 nm emission. To explain the relationship among the green emission, and the near- and mid-IR emissions, the energy level of Er^{3+} is demonstrated in Fig. 5(b). Ions of the $^4I_{15/2}$ state are excited to the $^4I_{11/2}$ state by ground state absorption (GSA) when the prepared samples are pumped by a 980 nm LD. On the one hand, some ions in the $^4I_{11/2}$ level undergo the energy transfer upconversion (ETU1) and excited stated absorption (ESA1) processes, thus contributing to the population of $^4F_{7/2}$ level. Afterward, the excited energy stored in the

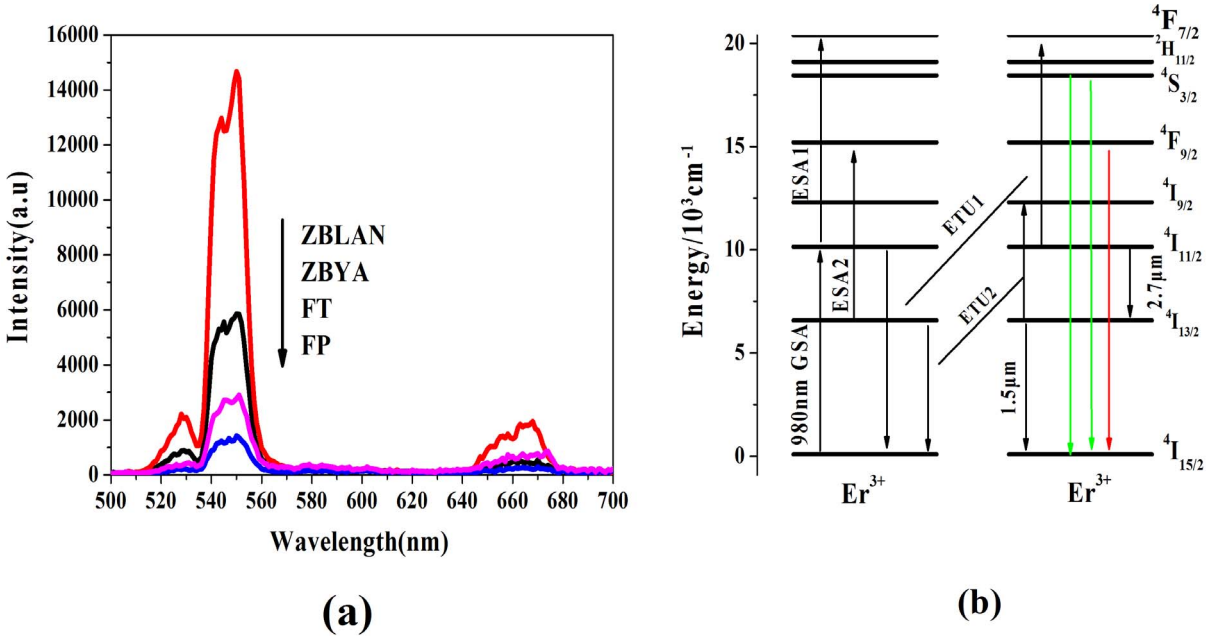

Figure 5 | **(a) Upconversion spectra of the present glasses, (b)Energy transfer sketch of Er^{3+}- doped glasses when pumped at 980 nm.**

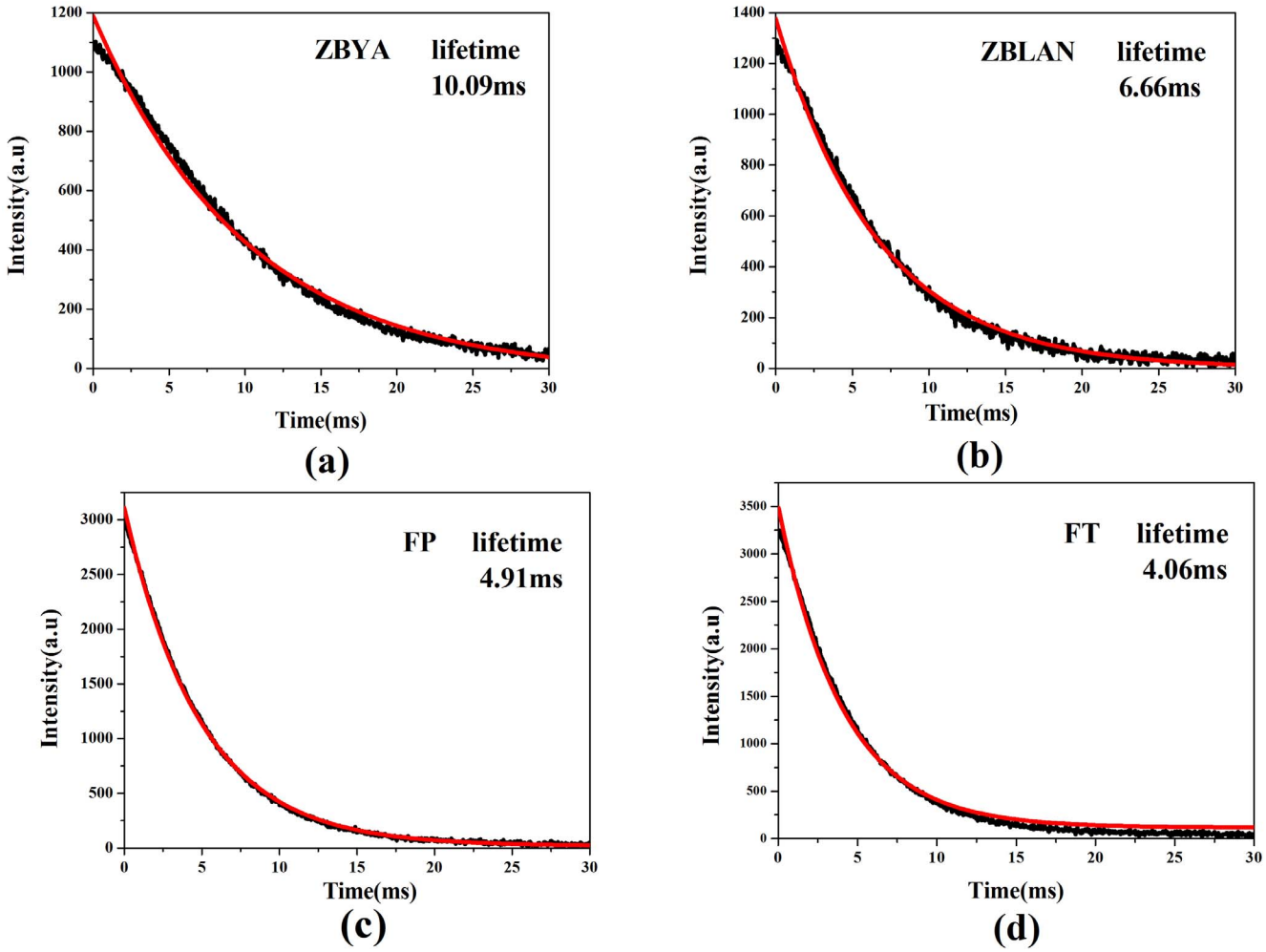

Figure 6 | Decay curves of 1.5 μm emission from the Er^{3+}- doped presented glasses.

$^4F_{7/2}$ level decays nonradiatively to the next- lower $^2H_{11/2}$ and $^4S_{3/2}$ levels. The green emission can be attributed to the Er^{3+}: $^4H_{11/2} \rightarrow {}^4I_{15/2}$ and $^4S_{3/2} \rightarrow {}^4I_{15/2}$ transitions. Some may have the chance to decrease to the lower $^4F_{9/2}$ energy through nonradiative decay, after which red emission (Er^{3+}: $^2F_{9/2} \rightarrow {}^4I_{15/2}$) occurs. On the other hand, ions in the $^4I_{11/2}$ level decay radiatively to the $^4I_{13/2}$ with 2.7 μm emission or nonradiatively to the $^4I_{13/2}$ level. Then the 1.5 μm emission occurs because of the $^4I_{13/2} \rightarrow {}^4I_{15/2}$ transition.

Fig. 6 shows the experimental decays of the Er^{3+}: $^4I_{13/2}$ level at room temperature of the present samples. The lifetime is an important factor for potential laser materials. All the samples show an exponential decay with lifetime of 10.09, 6.66, 4.91, and 4.06 ms, respectively, which are larger than those of tellurite glass (3.3 ms)[42], bismuth based glass (1.8 ms)[42], and borosilicate glass (2.0 ms)[43]. Difference exists between the values of lifetime that are measured and calculated because the measurement occurs at room temperature, but not at low temperature. The measured lifetimes of the fluorozirconte glasses are longer than those calculated ones owing to the serious self-absorption of the $^4I_{13/2}$ level. The fluorozirconate glasses possess longer lifetime of Er^{3+}: $^4I_{13/2}$ level but smaller intensity of 1.5 μm emission, which can be explained by that the lifetime is long enough to generate the ESA2 and ETU2 processes (as shown in Fig. 5(b)) and the ET between Er^{3+} ions.

Cross sections and emission parameters. Beer-Lambert[44] and Fuchtbauer-Ladenburg[45] equations are commonly used to calculate the cross section. The difference is that the former calculates the absorption cross section based on the absorption spectra firstly, whereas the latter calculates the emission cross section primarily based on the emission spectra and spontaneous transition probability. Both relate the absorption and emission cross sections through McCumber theory[36]. The equations are as follows:

$$\text{Beer}-\text{Lambert equation}: \ \sigma_a(\lambda) = \frac{2.303\log(I_0/I)}{Nl} \tag{3}$$

where $\log I_0/I$ is the absorbance from absorption spectrum, l is the thickness of the glass and N is the ion density.

$$\text{Fuchtbauer}-\text{Ladenburg equation}:$$

$$\sigma_e = \frac{\lambda^4 A_{rad}}{8\pi c n^2} \times \frac{\lambda I(\lambda)}{\int \lambda I(\lambda) d(\lambda)} \tag{4}$$

where λ is the wavelength, A_{rad} is the spontaneous transition probability, I(λ) is the emission spectrum, and n and c are the refractive index and light speed in vacuum respectively.

$$\text{McCumber equation}: \ \sigma_e(\lambda) = \sigma_a(\lambda)\left[\frac{Z_L}{Z_U}\right] e^{\left(\frac{E_{ZL}-hc\lambda}{kT}\right)} \tag{5}$$

where h is Planck's constant, K_B is the Boltzmann constant, T is the temperature, E_{zl} is the ground state manifold and the lowest stark level of the upper manifolds and Z_u and Z_l are partition functions of the lower and upper manifolds.

The absorption and emission cross sections of 1.5 μm for all present glasses are calculated using both methods. The results are shown in Table 3. The values calculated using BL method are larger than

Table 3 | Calculated emission and absorption cross section and effective line width around 1.5 and 2.7 μm of the present glasses obtained through both BL and FL equations

	Er^{3+}: $^4I_{13/2} \rightarrow {}^4I_{15/2}$							Er^{3+}: $^4I_{11/2} \rightarrow {}^4I_{13/2}$		
	σ_{abs} (BL) ($\times 10^{-21}$ cm^2)	σ_{em}(BL) ($\times 10^{-21}$ cm^2)	σ_{abs}(FL) ($\times 10^{-21}$ cm^2)	σ_{em}(FL) ($\times 10^{-21}$ cm^2)	$\Delta\lambda$ (nm)	τ_{cal} (ms)	τ_{exp} (ms)	σ_{em}(FL) ($\times 10^{-21}$ cm^2)	$\Delta\lambda$ (nm)	τ_{cal} (ms)
ZBYA	6.79	8.95	4.55	6.29	75.6	6.82	10.09	8.87	98.5	5.87
ZBLAN	5.79	7.26	4.84	6.56	77.3	6.44	6.66	10.03	90.8	5.50
FP	5.26	6.61	3.01	4.18	77.3	11.17	4.96	7.30	86.4	11.28
FT	5.23	6.98	4.01	5.56	73.6	8.15	4.06	8.81	88.1	7.17

those obtained using FL equation. Nevertheless, the same trend emerges, namely, the value of the absorption cross section is somewhat smaller than that of the emission cross section and the fluorozirconate glasses possess larger values compared with oxyfluoroaluminate glasses. To demonstrate the difference between the values calculated by the two equations, the cross sections at about 1.5 μm are described in Fig. 7 for the FP samples (similar spectra of other samples). The curves calculated from the FL equation seem smoother. FL may be more theoretically accurate because it is based on both the emission and the absorption spectra (the calculated spontaneous transition probability is based on the absorption spectra).

Full width at half maximum (FWHM) is a determiner for 1.5 μm laser materials[46]. The larger bandwidth of this transition is suitable for tunable lasers delivering relatively constant power over a wide wavelength range. The 1.5 μm emission from Er^{3+}- doped silicate glasses extensively used in the present study exhibit a narrow FWHM of about 30 nm, which limits their further applications[47]. The effective line width ($\Delta\lambda_{eff}$) is reportedly more accurate in estimating the bandwidth of this transition than FWHM because the emission band is slightly asymmetric[48]. The effective line width ($\Delta\lambda_{eff}$) is determined using the expression:

$$\Delta\lambda_{eff} = \int^{I(\lambda)d\lambda} / I_{max} \quad (6)$$

where I_{max} is the peak fluorescence intensity corresponding to λ_{eff} (the peak fluorescence wavelength). The $\Delta\lambda_{eff}$ values of 1.5 μm emission are presented in Table 3. The effective line width values in the present glasses are higher than those of silicate (34.8 nm)[49] and phosphate (46.0 nm)[49], making these fluoride glasses promising candidates for broadband amplifiers in WDM systems.

As known, a figure of merit (FOM) for the amplifier bandwidth is the product FWHM × σ_e[50], which can be inferred from Table 3. The products of the samples are much higher than those of ZBLAN (30 pm^2·nm) and Al/SiO_2 (25 pm^2·nm) glasses, which have been studied as potential EDFA hosts[51]. Meanwhile, the FOM for amplifier gain is usually defined as the product of stimulated emission cross section and lifetime ($\sigma_{em} \times \tau_{exp}$). As far as the material aspects are concerned, a larger product of $\sigma_{em} \times \tau_{exp}$ is desirable for an efficient fiber amplifier[52]. The product of ZBYA glass has an obvious advantage over Al/SiO_2 (5.5 pm^2·ms)[51]. These results show that Er^{3+}-doped fluoride glasses are promising candidate materials for 1.5 μm signal amplification.

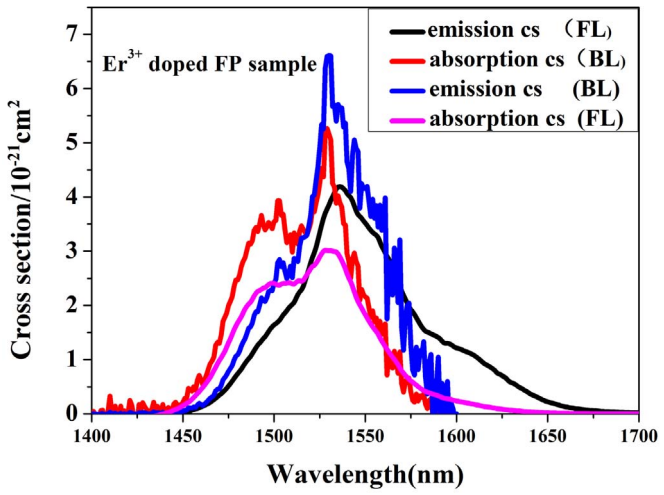

Figure 7 | The calculated emission and absorption cross section spectra around 1.5 μm emission of FP glass through both BL and FL equations.

Based on Fig. 4(b) and Equ.(3) to (6), the emission cross section and the effective line width of Er^{3+}: 2.7 μm are calculated, as shown in Table 3. The maximum emission cross section occurs at 2708 nm, and the values are above 7 × 10^{-21} cm^2 for all samples, which are higher than the reported values of 0.45 × 10^{-20} cm^2 in the YAG crystal[45], 0.53 × 10^{-20} cm^2 in the $LiYF_4$ crystal[53], 0.54 × 10^{-20} cm^2 in the ZBLAN glass[53], and 0.66 × 10^{-20} cm^2 in the chalcohalide glass[53].

Microparameters of energy transfer between Er^{3+} ions. To optimize the 1.5 and 2.7 μm laser systems, a quantitative understanding of the energy processes of Er^{3+}: $^4I_{13/2}$ level in the present glasses is required. The relevant energy transfer microparameters are quantitatively analyzed by applying the method developed by Forster and Dexter[54,55]. The probability rate of energy transfer between donor and acceptor can be described as

$$W_{DA} = \left(\frac{2\pi}{\hbar}\right)|H_{DA}|^2 S_{DA}^N \quad (7)$$

where $|H_{DA}|$ is the matrix element of the Hamiltonian perturbation between the initial and final states in the energy transfer process. S_{DA}^N is the overlap integral between the *m*-phonon emission line shape of donor ions (D) and *k*-phonon emission line shape of donor ions (A). For the case of weak electron-phonon coupling, S_{DA}^N can be approximated by

$$S_{DA}^N \approx \sum\nolimits_N e^{-(S_0^D S_0^A)}\left[\frac{(S_0^D S_0^A)^N}{N!}\right] S_{DA}(0,0,E)\partial_{(N,\Delta E/\hbar\omega_0)} \quad (8)$$

where S_{DA} (0, 0, E) represents the overlap integral between the zero-phonon line shape of donor emission ions and the absorption of acceptor ions. S_0^D, and S_0^A are the Huang-Rhys factor of donor and acceptor ions, respectively. The probability rate of energy transfer can be obtained using the following direct transfer equation:

$$W_{D-A}(R) = \frac{6cg_{low}^D}{(2\pi)^4 n^2 R^6 g_{up}^D}\sum\nolimits_{m=0}^{\infty} e^{-(2\bar{n}+1)S_0^m} \frac{S_0^m}{m!}(\bar{n}+1)^m \times \int \sigma_{emis}^D(\lambda_m^+)\sigma_{abs}^A(\lambda)d(\lambda) = \frac{C_{D-A}}{R^6} \quad (9)$$

Table 4 | Calculated interaction microscopic parameters $C_{D\text{-}A}$ for $^4I_{13/2}$ level in the present glasses. The number # of phonons necessary to assist the energy transfer process is also indicated along with its contribution (%)

Glass	N (No. of phonons) (%) phonon assisted		Transfer coefficient (10^{-39} cm^6/s)
ZBYA	0	1	3.99
	99.6%	0.4%	
ZBLAN	0	1	4.53
	99.7%	0.3%	
FP	0	1	1.94
	99.8%	0.2%	
FT	0	1	2.95
	99.8%	0.2%	

where $C_{D\text{-}A}$ is the energy transfer coefficient, R is the distance of separation between donor and acceptor, and the critical radius of the interaction can be obtained using the equation $R_C^6 = C_{D-A}\tau_D$, where τ_D is the intracenter lifetime of the excited level of donor. The expression for direct transfer (D-A) is then expressed by:

$$C_{DA} = \frac{6cg_{low}^{D}}{(2\pi)^4 n^2 g_{up}^{D}} \sum_{m=0}^{\infty} e^{-(2\bar{n}+1)S_0^m} \frac{S_0^m}{m!}(\bar{n}+1)^m \times \int \sigma_{emis}^{D}(\lambda_m^+)\sigma_{abs}^{A}(\lambda)d(\lambda) \quad (10)$$

Energy transfer properties of $^4I_{13/2}$ level in the present glasses are calculated using Eqs. (7) to(10) and are listed in Table 4. The results show that the energy transference of Er^{3+}: $^4I_{13/2}$ level in the present glasses scarcely needs phonon assistance. The results can explain why fluorozirconate glasses possess longer life time of 1.5 μm but less intensive 1.5 μm emission. The lifetime of Er^{3+}: $^4I_{13/2}$ is long enough for energy transfer between Er^{3+} ions. Accordingly, the intensity of 1.5 μm emission is weakened.

Conclusion

In conclusion, Er^{3+}- doped fluorozirconate (ZBYA) and oxyfluoroaluminate glasses have been prepared in this study. The DSC curves of these glasses show better thermal stability in resisting thermal damage at high pumping intensities compared with ZBLAN. The water treatment experiments show that ZBLAN exhibits serious weight loss and becomes opaque in the IR region. However, these samples demonstrate better resistance to water corrosion. Low OH^- absorption coefficient and phonon energy provide these glasses with potential for applications as laser materials. The high spontaneous transition probability and large emission cross section prove the intense near- and mid-infrared emissions. The energy transfer processes of Er^{3+} ions are discussed based on the upconversion, near- and mid- IR emissions spectra. The decay lifetime of Er^{3+}: $^4I_{13/2}$ is measured and the energy transfer microparameters between Er^{3+} ions are calculated. Therefore, the Er^{3+}- doped glasses in this study possess desirable thermal resistance properties and spectroscopic characteristics, which will be promising materials for infrared lasers and optical amplifiers.

1. Il'ichev, N. N. *et al.* Effective 2.5-μm ZnSe:Cr^{2+} laser with transverse laser pumping. *Laser Phy*, **20**, 1091–1094 (2010).
2. Wang, H. *et al.* Optical properties of Dy^{3+} ions in sodium gadolinium tungstates crystal. *J. Lumin.* **126**, 452–458 (2007).
3. Lakshminarayana, G. & Qiu, J. Photoluminescence of Pr^{3+}, Sm^{3+} and Dy^{3+}-doped SiO_2–Al_2O_3–BaF_2–GdF_3 glasses. *J. Alloys Com.* **476**, 470–476 (2009).
4. Burtan, B. *et al.* Optical properties of Nd^{3+} and Er^{3+} ions in TeO_2–WO_3–PbO–La_2O_3 glasses. *Opt Mater.* **34**, 2050–2054 (2012).
5. Nawaz, F. *et al.* Spectral investigation of Sm^{3+}/Yb^{3+} co-doped sodium tellurite glass. *Chin. Opt. Lett.* **11**, 061605 (2013).
6. Xu, Y. *et al.* Nanocrystal-enhanced near-IR emisssion in the bismuth-doped chalcogenide glasses. *Chin. Opt. Lett.* **11**, 041601 (2013).
7. Ming, C. *et al.* Tm^{3+}/Er^{3+}/Yb^{3+} tri-doped TeO_2-PbF_2-AlF_3 glass for white-emitting diode. *Opt Commun.* **304**, 80–82 (2013).
8. Rayappan, I. A. & Marimuthu, K. Structral and lumilnescence behavior of the Er^{3+} doped alkali fluorobarate glsses. *J. Non-Cryst Solids.* **367**, 43–50 (2013).
9. Guo, R. *et al.* Optical transition probabilities of Er^{3+} ions in $La_2CaB_{10}O_{19}$. *Chem Phys Lett.* **416**, 133–136 (2005).
10. Zhan, H. *et al.* Intense 2.7 μm emission of Er^{3+} -doped water-free fluorotellurite glasses. *Opt. Lett.* **37**, 3408–3410 (2012)
11. Li, X. *et al.* Emission enhancement in Er^{3+}/Pr^{3+}-codoped germanate. *Chin. Opt. Lett.* **11**, 121601 (2013).
12. Maheshvaran, K. *et al.* Strucural and luminescence studies on Er^{3+}/Yb^{3+} co-doped boro-tellurite glasses. *J. Alloys Com.* **561**, 142–150 (2013).
13. Ter-Gabrielyan, N. *et al.* Ultralow quantum-defect eye-safe Er: Sc_2O_3 laser. *Opt. Lett.* **33**, 1524–1526 (2008).
14. Wei, C. *et al.* Passively continuous-wave mode-locked Er^{3+}-doped ZBLAN fiber laser at 2.8 μm. *Opt. Lett.* **37**, 3849–3851 (2012).
15. Artjushenko, V. G. *et al.* Medical applications of MIR-fiber spectroscopi probes. *Biochemical and Medical Sensors.* **2085**, 137–142 (1993).
16. Guo, C. *et al.* High-power and widely tunable Tm-doped fiber laser at 2 μm. *Chin. Opt. Lett.* **10**, 091406 (2012)
17. Guo, Y. *et al.* Intense 2.7 μm emission and structural origin in Er^{3+}-doped bismuthate (Bi_2O_3-GeO_2-Ga_2O_3-Na_2O) glass. *Opt. Lett.* **37**, 268–270 (2012).
18. Said Mahraz, Z. A. *et al.* Concentration dependent luminescence quenching of Er^{3+}-doped Zinc boro-tellurite glass. *J. Lumin.* **144**, 139–145 (2013).
19. Yin, D. *et al.* Enhancement of the 1.53 μm fluorescence and energy transfer in Er^{3+}/Yb^{3+}/Ce^{3+} tri-doped WO_3 modified tellurite-based glass. *J. Alloys Com.* **581**, 534–541 (2013).
20. Zhao, G. *et al.* Effcient 2.7 μm emission in Er^{3+}-doped bismuth germanate glass pumped by 980nm laser diode. *Chin. Opt. Lett.* **10**, 091601–091603 (2012).
21. Guo, Y. *et al.* Er^{3+}-doped fluoro-tellurite glass: A new choice for 2.7 μm lasers. *Mater Lett.* **80**, 56–58 (2012).
22. Lavin, V. *et al.* Site selective study in Eu^{3+}-doped fluorozirconate glasses. *J. Lumin.* **72**, 437–438 (1997).
23. Dakui, D. & Fuding, M. Glass formation and crystallization in AlF_3-YF_3-BaF_2-CaF_2-MgF_2. *J. Non-Cryst Solids.* **168**, 275–280 (1994)
24. Yasui, I. *et al.* The effect of addition of oxides on the crystallization behavior of aluminum fluoride-base glasses. *J. Non-Cryst Solids.* **140**, 130–133 (1992).
25. Rigout, N. *et al.* Chemical and physical compatibilities of fluoride and fluorophosphate glasses. *J. Non-Cryst Solids.* **184**, 319–323 (1995).
26. Choi, Y. G. *et al.* Emission properties of the Er^{3+}:$^4I_{11/2} \rightarrow {}^4I_{13/2}$ transition in Er^{3+}- and Er^{3+}/Tm^{3+} -doped Ge-Ga-As-S glasses. *J. Non-Cryst Solids.* **278**, 137–144 (2000).
27. Wang, X. *et al.* Spectroscopic properties of thulium ions in bismuth silicate glass. *Chin. Opt. Lett.* **10**, 101601 (2012).
28. Tian, Y. *et al.* 1.8 μm emission of highly thulium doped fluorophosphate glasses. *J. Appl Phys.* **108**, 083504 (2010).
29. Xu, R. *et al.* 2.05 μm emission properties and energy transfer mechanism of germanate glass doped with Ho^{3+}, Tm^{3+}, and Er^{3+}. *J. Appl Phys.* **109**, 053503 (2011).
30. Lebullenger, R. *et al.* Systematic substitutions in ZBLA and ZBLAN glasses. *J. Non-Cryst Solids.* **161**, 217–221 (1993).
31. Rigout, N. *et al.* Chemical and physical compatibilities of fluoride and fluorophosphate glasses. *J. Non-Cryst Solids.* **184**, 319–323 (1995).
32. Frischat, G. H. *et al.* Chemical stability of ZrF_4- and AlF_3- based heavy metal fluoride glasses in water. *J. Non-Cryst Solids.* **284**, 105–109 (2001).
33. Yu, X. *et al.* Infrared spectrum estimaion for maximum phonon energy in optical glasses. *J. Dalian Polytechnic University.* **27**, 155–157 (2008).
34. Tian, Y. *et al.* Optical absorption and near infrared emissions of Nd^{3+} doped fluorophosphate glass. *Spectrochimica acta. Part A, Molecular and biomolecular spectroscopy.* **98**, 355–358 (2012).
35. Jiang, X. *et al.* Fluorogermanate glass with reduced content of OH^- groups for infrared optics. *J. Non-Cryst Solids.* **355**, 2015–2019 (2009).
36. Huang, F. *et al.* Highly Er^{3+}-doped ZrF_4-based fluoride glasses for 2.7 μm laser materials. *Appl opt.* **52**, 1399–1343 (2013).

37. Ding, J. *et al.* Effect of P_2O_5 addition on the structural and spectroscopic properties of sodium aluminosilicate glass. *Chin. opt. lett.* **10**, 071602 (2012)
38. Tian, Y. *et al.* 2 μm Emission of Ho^{3+}-doped fluorophosphate glass sensitized by Yb^{3+}. *Opt Mater.* **32**, 1508–1513 (2010).
39. Zhang, Y. *et al.* Spectroscopic properties of Dy^{3+}:$Bi_4Si_3O_{12}$ single crystal. *J. Alloys Com.* **582**, 635–639 (2014).
40. Shinn, M. D. & Sibley, W. A. Optical transitions of Er^{3+} ions in fluorozirconate glass. *Phys. Rev.* **27**, 6635–6648 (1983).
41. Guo, H. N. *et al.* Visible Upconversion in Rare Earth Ion-Doped Gd_2O_3 Nanocrystals. *J Phys Chem B.* **108**, 19205–19209 (2004).
42. Rolli, R. *et al.* Eribium doped tellurite glasses with high quantum efficiency and broadband stimulated emission cross section at 1.5 μm. *Opt Mater.* **21**, 743–748 (2003).
43. Yang, J. *et al.* Mixed heavy metal effect on emission properties of Er^{3+}-doped borosicilate glasses. *Chin. Opt. Lett.* **1**, 294–295 (2003).
44. Xu, R. *et al.* Spectroscopic properties of 1.8 μm emission of thulium ions in germanate glass. *Appl Phys B.* **102**, 109–116 (2010).
45. Zhuang, X. *et al.* Enhanced emission of 2.7 μm from Er^{3+}/Nd^{3+}-codoped $LiYF_4$ single crystals. *Materials Science and Engineering: B.* **178**, 326–329 (2013).
46. Jha, A. *et al.* Rare-earth ion doped TeO_2 and GeO_2 glasses as laser materials. *Progress in Materials Science.* **57**, 1426–1491 (2012).
47. Ohishi, Y. *et al.* Gain characteristic of tellurite-based erbium doped fiber amplifiber. *Opt Letters.* **23**, 274–276 (1998)
48. Sasikala, T. *et al.* Spectroscopic properties of Er^{3+} and Ce^{3+} co-doped tellurite glasses. *J. Alloys Com.* **542**, 271–275 (2012).
49. Ding, Y. *et al.* Spectral properties of erbium-doped lead halotellurite glasses. *Proc. SPIE.* 166–173 (2000).
50. Jayasimdadri, M. *et al.* Er^{3+}-doped tellurofluorophoaphate glasses for laser and optical ampliers. *J. Phys. Condens.* **17**, 7705–7715 (2005).
51. Shen, S. *et al.* Tellurite glasses for broadband amplifiers and integrated optics. *J. Am. Cream. Soc.* **85**, 1391–1395 (2002).
52. Wei, K. *et al.* Pr^{3+}- doped Ge-Ga-S glasses for 1.3 μm optical fiber amplifiers. *J. Non-Cryst Solids.* **182**, 257–261 (1995).
53. Lin, H. *et al.* Enhanced mid-infrared emisssions of Er^{3+} at 2.7 μm via Nd^{3+} sensitization in chalcohalide glass. *Opt Letters.* **36**, 1815–1817 (2011).
54. Xu, R. *et al.* 2.0 μm emission properties and energy transfer processes of Yb^{3+}/Ho^{3+} codoped germanate glass. *J. Appl Phys.* **108**, 043522 (2010)
55. Tian, Y. *et al.* Intense 2.0 μm emission properties and energy transfer Ho^{3+}/Tm^{3+}/Yb^{3+} doped fluorophosphate glasses. *J. Appl Phys.* **110**, 033502 (2011).

Author contributions

F.H. wrote the main manuscript text and coauthor X.L. checked up. D.C. and L.H. are responsible for the experiment. All authors reviewed the manuscript.

Additional information

Competing financial interests: The authors declare no competing financial interests.

How to cite this article: Huang, F.F., Liu, X.Q., Hu, L.L. & Chen, D.P. Spectroscopic properties and energy transfer parameters of Er^{3+}- doped fluorozirconate and oxyfluoroaluminate glasses. *Sci. Rep.* **4**, 5053; DOI:10.1038/srep05053 (2014).